J Comp Physiol A (2011) 197:153–165
DOI 10.1007/s00359-010-0596-3

ORIGINAL PAPER

Response properties of visual neurons in the turtle nucleus isthmi

Debajit Saha · David Morton · Michael Ariel · Ralf Wessel

Received: 8 July 2010 / Revised: 5 October 2010 / Accepted: 8 October 2010 / Published online: 22 October 2010
© Springer-Verlag 2010

Abstract The optic tectum holds a central position in the tectofugal pathway of non-mammalian species and is reciprocally connected with the nucleus isthmi. Here, we recorded from individual nucleus isthmi pars parvocellularis (Ipc) neurons in the turtle eye-attached whole-brain preparation in response to a range of computer-generated visual stimuli. Ipc neurons responded to a variety of moving or flashing stimuli as long as those stimuli were small. When mapped with a moving spot, the excitatory receptive field was of circular Gaussian shape with an average half-width of less than 3°. We found no evidence for directional sensitivity. For moving spots of varying sizes, the measured Ipc response-size profile was reproduced by the linear Difference-of-Gaussian model, which is consistent with the superposition of a narrow excitatory center and an inhibitory surround. Intracellular Ipc recordings revealed a strong inhibitory connection from the nucleus isthmi pars magnocellularis (Imc), which has the anatomical feature to provide a broad inhibitory projection. The recorded Ipc response properties, together with the modulatory role of the Ipc in tectal visual processing, suggest that the columns of Ipc axon terminals in turtle optic tectum bias tectal visual responses to small dark changing features in visual scenes.

D. Saha (✉) · D. Morton · R. Wessel
Department of Physics, Washington University,
St. Louis, MO 63130-4899, USA
e-mail: dsaha@physics.wustl.edu

M. Ariel
Department of Pharmacological and Physiological Science,
Saint Louis University School of Medicine, St. Louis,
MO 63104-1004, USA

Keywords Nucleus isthmi · Tectum · GABAergic inhibition · Vision · Receptive field

Abbreviations

ACh	Acetylcholine
GABA	Gamma-aminobutyric acid
Imc	Isthmi pars magnocellularis
Ipc	Isthmi pars parvocellularis
PBN	Parabigeminal nucleus
RGC	Retinal ganglion cell
SFGS	Stratum fibrosum et griseum superficiale
SGC	Stratum griseum centrale
SGP	Stratum griseum periventriculare

Introduction

The nucleus isthmi (parabigeminal nucleus) is a visually responsive midbrain structure in vertebrates (Sherk 1978, 1979a; Yan and Wang 1986; Northmore 1991; Wang and Frost 1991; Wiggers and Roth 1991; Cui and Malpeli 2003; Northmore and Gallagher 2003; Gallagher and Northmore 2006; Maczko et al. 2006; Li et al. 2007; Caudill et al. 2010) that influences visual processing by direct modulation of tectal circuits (Wang et al. 1995; Wang et al. 2000; Winkowski and Gruberg 2002; Dudkin and Gruberg 2003; Wang 2003; Marín et al. 2007). This modulation is mediated by reciprocal connections between the nucleus isthmi and optic tectum (Graybiel 1978; Gruberg and Udin 1978; Sereno and Ulinski 1987; Powers and Reiner 1993; Wang et al. 2004, 2006).

The turtle magnocellular isthmic complex contains two cytoarchitectonically distinct isthmic nuclei (Fig. 1), which

receive sensory information from the ipsilateral optic tectum (Sereno and Ulinski 1987; Powers and Reiner 1993). In order to make comparisons with avian systems we have adopted the nomenclature consistent with the avian isthmotectal system (Wang et al. 2004, 2006) following the recommendation of Powers and Reiner (Powers and Reiner 1993). When we refer to the two isthmic nuclei as the pars parvocellularis (Ipc) and the pars magnocellularis (Imc), these correspond to the caudal and rostral nucleus isthmi pars magnocellularis, respectively, from earlier turtle literature (Sereno and Ulinski 1987). Retinal ganglion cell (RGC) axons terminate in the superficial layers of the tectum (Fig. 1) where they innervate the radial, narrow dendrites of the tectal stratum griseum periventriculare (SGP) neurons (Schechter and Ulinski 1979). The axons of SGP neurons project to the Ipc and Imc nuclei (Kunzle and Schnyder 1984). In the Imc, neurons have large, sparsely branched dendritic fields overlapped by local axon collaterals. The axons of Imc neurons nontopographically project to both the deeper layers of the tectum and to the Ipc (Sereno and Ulinski 1987). In the Ipc, neurons have medium-sized, elongated somata, flattened bipolar dendritic fields, and axons that project topographically back to the tectum. Each Ipc axon terminates as a compact swarm of boutons within a cylinder about 150 μm in diameter and 400 μm tall, placed mainly in the upper tectal layers, where it spans less than one percent of the tectal surface (Sereno and Ulinski 1987). The topographically-organized, columnar Ipc axon terminals spatially overlap with the RGC axons and the SGP neuron dendrites (Fig. 1).

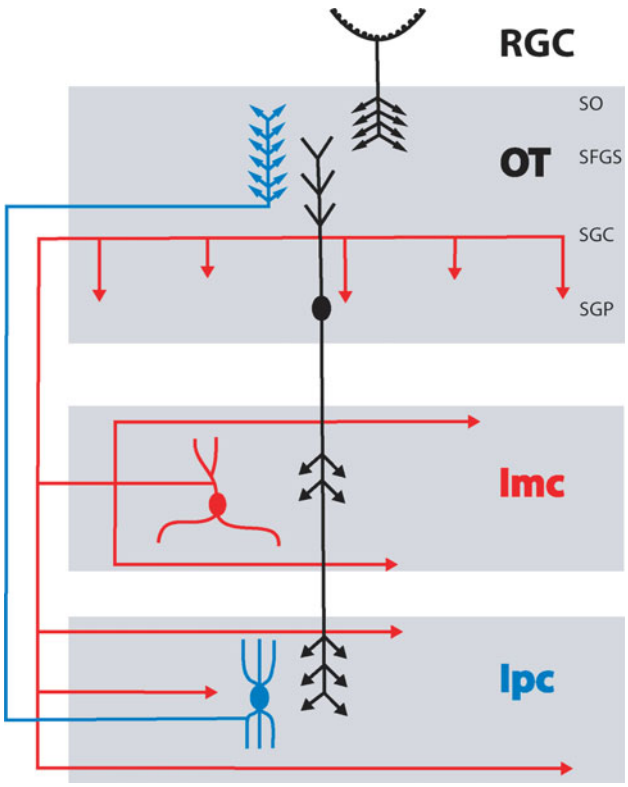

Fig. 1 Schematic drawing of the turtle isthmotectal feedback circuitry. Neurons in the optic tectum (OT) with somata in the SGP layer receive RGC inputs at their narrow apical dendrites in the SFGS layer. These glutamatergic SGP neurons (*black*) project to the two isthmic nuclei: pars parvocellularis (Ipc) and pars magnocellularis (Imc). The GABAergic Imc neurons (*red*) have large, sparsely branched dendritic fields, and axons that project nontopographically to the Ipc and to the deeper tectal layers (SGC, SGP) in addition to local axon collaterals. The cholinergic Ipc neurons (*blue*) have flattened bipolar dendrites and project topographically to the upper layers of ipsilateral tectum. We use the revised nomenclature, Ipc and Imc, for isthmic nuclei, which is consistent with the nomenclature in the avian isthmotectal system

Cholinergic isthmic neurons (turtle: Desan et al. 1984; Powers and Reiner 1993; frog: Gruberg and Udin 1978; Winkowski and Gruberg 2002; Dudkin et al. 2007; bird: Sorenson et al. 1989; Medina and Reiner 1994; mammal: Graybiel 1978; Sherk 1979b; Hall et al. 1989) provide a major source of acetylcholine (ACh) to the optic tectum (superior colliculus). Although the cholinergic neurons are hypothesized to be modulators of tectal activity (Goddard et al. 2007), the information represented in the spatiotemporal pattern of ACh release is largely unknown. In general, the extensive studies of cholinergic modulation in the brain have focused largely on the postsynaptic effect of ACh release (McCormick 1993; Lucas-Meunier et al. 2003; Metherate 2004; Lucas-Meunier et al. 2009). Cholinergic Ipc neurons, being visually responsive and reciprocally connected exclusively to the tectum, are an ideal system to study both spatiotemporal pattern of ACh release and its postsynaptic effect on tectal neurons. While this study does not address the postsynaptic effects of ACh in the optic tectum, an understanding of the visual responses of Ipc neurons is a necessary first step in the direction of correlating visual stimulation with spatiotemporal ACh release.

To investigate the visual response properties of the Ipc, we conducted extracellular recordings from Ipc neurons during visual stimulation to the contralateral retina (Fig. 2) in a turtle eye-attached whole-brain preparation (Kriegstein 1987; Rosenberg and Ariel 1990). Apart from preserving the long-range visual circuitry, this whole-brain preparation simplifies accessibility to the Ipc and mitigates the primary in vivo complications such as heart beat vibrations and the lack of control of the extracellular media. We presented a wide variety of visual stimuli (see "Methods") and found that the Ipc responds strongly to small stimuli preferably dark compared with the background. Ipc responses to static stimuli show significant temporal adaptation. For dynamic stimuli, the Ipc responses are tuned to the stimulus size with no directional preference.

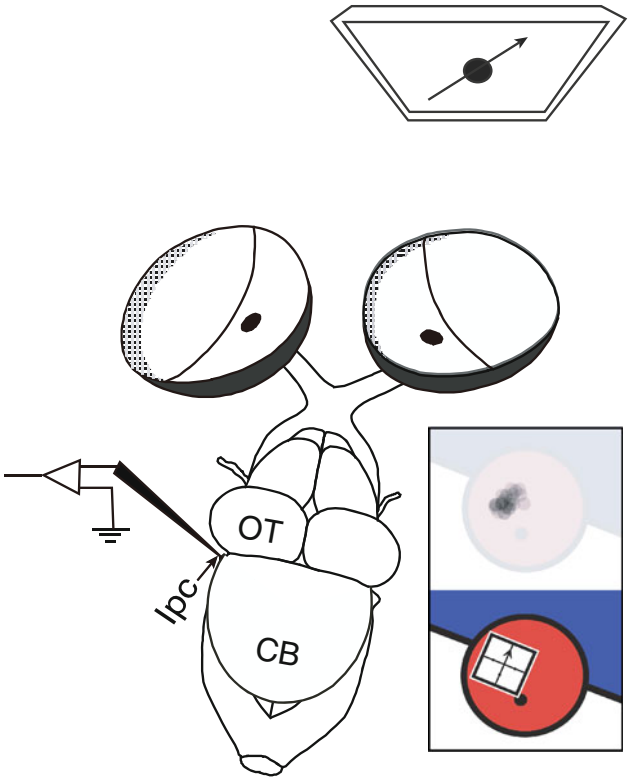

Fig. 2 Schematic drawing of a dorsal view of the turtle whole-brain preparation with the eye-cups attached and the telencephalon removed. Computer-generated visual stimuli are presented on a monitor (*moving black spot*) and are projected with appropriate optics (not shown) onto the retinal eye-cup. Surface landmarks guide the placement of microelectrodes for extracellular and blind-patch whole-cell recordings from Ipc. *Inset* The monitor-to-eye-cup projection and the presentation of visual stimuli. *Top* evaluating a responsive area in the visual field with small moving spot stimuli. *Bottom* defining a stimulation coordinate system (*white square*) covering the entire responsive area

Methods

Surgery

Eighteen adult red-ear turtles (*Trachemys scripta elegans*, 12–15 cm carapace length) were used in this study. Following cryanesthesia (>15 min of hypothermia in ice water), rapid decapitation and then cannulation were performed on neck vasculature to infuse cold saline to rinse out cranial blood. Within 20 min of decapitation, the telencephalon was removed. The eye was kept attached to the brainstem but freed from its orbits by cutting the conjunctiva and extraocular muscles. The eye was then hemisected and drained of its vitreous. The dura surrounding the brain was removed, as was the pia covering lateral mesencephalon. The preparation was then transferred to the superfusion chamber positioned on an air table with the eye-cup beneath a focusing lens. The preparation was bathed in physiological media (in mM; 85 NaCl, 2 KCl, 2 $MgCl_2$, 45 $NaHCO_3$, 20 D-glucose, 3 $CaCl_2$ bubbled with 95% O_2 and 5% CO_2), adjusted to pH 7.4 at room temperature.

Extracellular recordings

Extracellular recordings from Ipc neurons were achieved with tungsten microelectrodes (A-M Systems, parylene-C insulated, 250 μm core diameter, 12° tapered tip) of 1 MΩ impedance (measured at 1 kHz, 0.1 nA *p-p* current). Since the Ipc is a surface structure, its location was identified by a characteristic protrusion just caudal of the optic tectum (Fig. 2). To find a responsive recording site, the microelectrode was advanced smoothly into the Ipc (100–400 μm), using a hydraulic drive (FHC 50-12-9 Manual Drum Drive Unit) while the search stimulus (see below) was focused on the retina of the contralateral eye-cup. The voltage traces were obtained using a differential AC amplifier (A-M Systems, Model 1800). The signal was passed through a 300–5,000 Hz analog band-pass filter and then sampled at 10 kHz (PCI-MIO-16E-4) using a LabView-controlled data acquisition system (National Instruments). Recordings were continuously monitored using an audio monitor (AM Systems 3300) and an oscilloscope (Tektronix TDS 210).

Visual stimulation

Visual stimuli were created by a computer and delivered with an LCD monitor (Samsung 19 in., 1,440 × 900 pixels, contrast ratio = 20,000:1, response time = 2 ms). The image on the monitor was projected onto the retinal surface of the hemisected eye-cup with a converging lens system (Fig. 2). A monitor pixel corresponded to 7 μm on the retina or ~0.08° of visual angle (Northmore and Granda 1991; Ariel and Kogo 2001). Stimuli were created using *psychopy*, an open-source psychophysics module written for the Python programming language (Peirce 2008).

Eye-cup layout

Software tools were written to allow the experimenter to characterize the projection of the computer screen onto the retina. A computer game pad was used to control the measurements of size and position of the eye-cup interactively, relative to the monitor. The eye-cup parameters, including the position and orientation of the visual streak, and the size and position of the optic disk were documented. An image based on these parameters (Fig. 2, bottom inset) was projected onto the eye cup preparation (in the recording chamber) allowing for interactive adjustments. The visual streak represents a high-density of

photoreceptors and RGCs in the turtle retina (Brown 1969). It is identified by visual inspection as a faint white linear structure along the nasal-temporal direction of the eye.

Search stimulus

The search stimulus consisted of 5–8 black spots of different sizes (diameter 2–8°) moving pseudo-randomly on a white background with different directions and speeds (2–5°/s). The spots moved in a straight line until they reached the edge of the eye cup region whereupon they randomly changed direction but not speed or size. Unless specified otherwise, the default computer screen background was white in a darkened room.

Stimulation coordinate system

To define the stimulation coordinate system, we monitored neural activity while a black spot moved on the screen, starting outside the eye cup region. The movement and size of the spot was controlled by a computer mouse. As the spot moved towards the eye cup center, single/multi unit responses were audibly detected at some locations with the use of an audio monitor. The spot locations and sizes were saved at the onset of a response by clicking the mouse. After many such identifications of responses, an image of all the response-triggering spots overlaid on each other was generated (Fig. 2, top inset). This image was used as a guide to define a stimulation coordinate system that was about twice the size of the active area and oriented parallel to the visual streak (white square in Fig. 2, bottom inset). All experimental stimuli were subsequently scaled and rotated using this normalized stimulation coordinate system, giving us the ability to generate a whole set of stimuli which can be presented independently of the particulars of each monitor-to-eye-cup projection setup. The nasal retina or temporal visual field parallel to the visual streak was defined 0° (180°) in the right (left) eye. The superior and inferior visual fields were defined as 90° and 270°, respectively, for both eyes.

Visual stimuli

Various stimuli, both static and moving were shown from a pool of computer-generated stimuli. During an experiment, stimuli were shown time-locked with the data acquisition. The data acquisition system sent a 5-V trigger pulse to the stimulus computer's parallel port, triggering the display of the stimulus. With the video card (ASUS EN8600GT, 256 MB), the *psychopy* codes maintained sub-millisecond frame-rendering precision. Interstimulus intervals of at least 30 s were maintained between different sets of stimuli.

To study the Ipc visual response properties to different stimuli, seven different types of stimuli were used. (S1) Black moving spot on white background—a small spot of diameter 6–8° moved at about 6–8°/s radially through the center of the stimulation coordinates in eight directions (0, 45,…,315 degrees relative to the visual streak) pseudo randomly. There was ≥500 ms wait between different directions being presented within the stimulus set. (S2) White moving spot on black background—this set of stimuli was identical to stimulus S1 except that the contrast was inverted. (S3) Black leading edge on white background—a bar moved along its long axis so that only the leading edge crossed the screen. The short axis was the same size as the diameter of spots in stimuli S1 and S2, likewise for the speed. (S4) Randomly changing check pattern—the stimulation coordinate system was divided into a 4 × 4 grid, and each grid space pseudo-randomly displayed white or black with equal probability. Each grid space (check) was about 8° square. All 16 checks were updated every 10 frames (168 ms). This stimulus was displayed for 25 s. (S5) Drifting sinusoidal grating—a grating was displayed with motion perpendicular to the visual streak. The spatial frequency was 0.02 cycles/degrees, and the temporal frequency was 1 Hz. The stimulus was displayed for 25 s. (S6) Flashing black spot on white background—a small spot of diameter 6–8° was displayed for 5 s in the center of the stimulation coordinate system. (S7) Whole screen flash from white to black—the entire screen was set to display black for 5 s. Note that except for S2, the computer screen background was white before and after the trials of stimuli.

Extracellular data analysis

To determine the number of active units at the recording site, sample recordings were analyzed with *waveclus*, a spike-sorting algorithm based on spike detection and sorting using wavelets and superparamagnetic clustering (Quiroga et al. 2004). Single units were isolated using criteria that included a well-defined spike shape with no kinks in the standard deviation of all classified spikes and a refractory period of 2 ms in the interspike interval distribution. Only single-unit responses were used for the analysis. For each experiment we obtained recordings for at least three trials, with exceptions noted in the figure captions.

Difference-of-Gaussians analysis

The stimulus size-response profile of Ipc neurons were analyzed using the Difference-of-Gaussians model (Rodieck 1965; DeAngelis et al. 1994; Sceniak et al. 1999), which assumes the linear and independent sum of two concentric Gaussians, excitatory and inhibitory, yielding

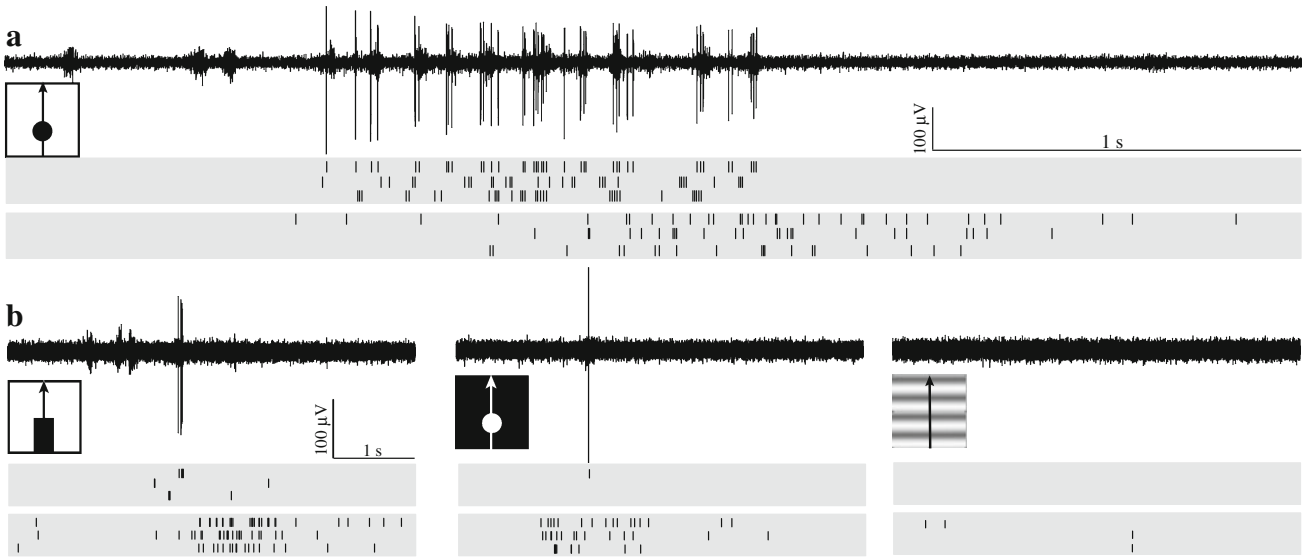

Fig. 3 Stimulus-selective visual responses of Ipc neurons. **a** Responses of two single-unit Ipc neurons to a *black spot* moving perpendicular to the visual streak. Schematic of the stimulus is shown at the left of the respective voltage trace. The *square box* represents the stimulation coordinate system, which covers the entire responsive area of the unit and is aligned parallel to the visual streak. The direction of stimulus movement is indicated by the *arrow*. Top to bottom, raw voltage trace, raster of three trials of one unit and raster of another single-unit from a different recording site. The *gray boxes* indicate the duration of stimulus movement. Spot diameter: 7°, 8°; speed: 7°/s, 8°/s, respectively, for two units. **b** Responses to other moving stimuli for the same units shown in (**a**). From left to right, moving leading edge, moving *white spot* (same dimension and speed as of *black spot* in **a**) and drifting sine grating (spatial frequency 0.02 cycles/degrees, temporal frequency 1 Hz)

the net response to the stimulus. We used moving spots (stimulus S1) of different sizes to study the stimulus size tuning of Ipc neurons. The assumption was made that only the spot's leading edge is generating the Ipc response. With this assumption, for a linear sweep of a moving spot of radius s, the net response $R(s)$ follows the relation

$$R(s) = R_0 + K_e \int_{-a/2}^{a/2} e^{-(2x/a)^2} dx \int_{-s}^{s} e^{-(2y/a)^2} dy - K_i \int_{-b/2}^{b/2} e^{-(2x/b)^2} dx \int_{-s}^{s} e^{-(2y/b)^2} dy$$

where the parameters K_e and K_i represent the strength of excitatory and inhibitory receptive fields, respectively, while a and b represent the spatial extent of excitatory and inhibitory Gaussian receptive fields. The baseline activity R_0 is assumed to be zero due to low (<1 Hz) spontaneous activity of Ipc units. Notice that the equation is equivalent to one commonly used for flashing spot stimuli of different radius with an additional constant multiplicative factor due to the integration of the whole Gaussian profile along one direction.

Blind-patch whole-cell recording

For blind-patch whole-cell recordings from Ipc neurons, patch pipettes were fabricated on a Flaming-Brown horizontal puller (P-97, Sutter Instruments) from Corning #7052 glass capillary tubing (OD 1.5 mm, ID 0.86 mm) to yield 5–8 MΩ pipette resistance. The pipette solution for ruptured patch recordings contained (in mM) 117 KMeS-O_4, 5 KCl, 5 NaCl, 1.2 $MgCl_2$, 10 HEPES, 5 EGTA; pH 7.3; with osmolarity 260 mOsMol. Pipette solutions were filtered before use. Electrodes were advanced through the Ipc with a motorized micromanipulator (MP-285, Sutter Instruments) while maintaining a constant positive pressure. Electrode resistance was monitored continuously by applying short current pulses (Axoclamp 900 amplifier; −1.0 nA, 10 ms duration, 10 Hz). An increase of the resulting voltage pulse height (an increase in series resistance) was observed as the pipette tip approached a cell membrane. The pipette was advanced until the series resistance increased by about 10 MΩ. Current was then reduced to −0.1 nA and the positive pressure was reversed to a small negative pressure by pulling gently on a syringe plunger. This gentle suction was applied until the pipette formed a GΩ seal. Additional brief suction was applied to rupture the patch of membrane within the pipette. The pipette capacitance was compensated by the amplifier's circuitry and the access resistance was monitored. Analog data were low-pass filtered (4-pole Butterworth) at 1 kHz, digitized at 10 kHz, stored and analyzed on a PC equipped with a PCI-MIO-16E-4 and LabView software.

For stimulation of presynaptic Imc axons, a concentric, bipolar tungsten electrode (tip diameter = 4 µm; core

diameter = 76 μm) was lowered into deep tectal layers (Figs. 1, 10). A 200-μA current pulse of 0.5 ms duration was used to stimulate Imc axons in deep tectal layers while recording from the Ipc neuron intracellularly. No visual stimuli were applied during intracellular recordings.

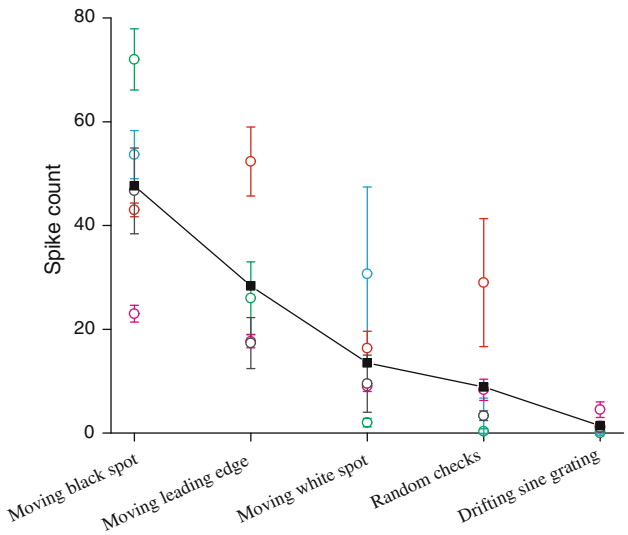

Fig. 4 Population study of single-unit Ipc responses to spatiotemporally changing stimuli. Presented are 5 single-units, collected from five sites of four different brains. Responses for Ipc neurons to different stimuli are quantified by the average spike count, which is the number of spikes for the first 5 s after stimulus onset and averaged over multiple trials. Small moving stimuli; *black spot*, *black leading edge,* and *white spot* are presented in the stimulus coordinate system of each unit (S1, S3, S2, respectively, see "Methods"). Spot diameter, edge width, and speed are kept constant for one unit but varied slightly from unit to unit (spot diameter/edge width 6–8°, speed 6–8°/s). For each unit the maximum value of average spike count along any one direction (out of 8) is plotted for each small moving stimulus. The cyan unit was not tested for leading edge stimuli. *Error bars* represent SD for multiple trials ($m = 2$ for *white moving spot* stimulus of *blue* and *magenta* units, $m = 3$ for all others). For broad spatiotemporally changing stimuli; random flashing checkerboard and drifting sine grating (S4, S5), the average spike counts are plotted with the SD values. The *black squares* indicate the average response of all single-units for any given stimulus. The *green* and *red* circles indicate the Ipc units shown in Fig. 3

Results

Stimulus selectivity

To evaluate to what extent Ipc visual response properties are stimulus specific, we conducted extracellular recordings while showing different stimuli in a pseudo-random order. Stimuli were shown to the contralateral eye of the recorded Ipc neuron. A continuously illuminated white screen elicited almost no response (mean = 0.1 Hz, SD = 0.2 Hz, $n = 8$ units). However, a dark spot (diameter 6–8°) on a white screen moving through the center of the excitatory receptive field of an Ipc neuron at a speed of 6–8°/s elicited strong spiking responses (Figs. 3a, 4; spike count 23–72, $n = 5$ units). For all stimuli and Ipc units tested, responses are quantified as the average spike count during the first 5 s of stimulus presentation (Fig. 4). The Ipc response was somewhat reduced when the dark spot was replaced by a moving leading edge of similar width and speed (spike count 17–52, $n = 4$ units) or when a white spot moved on a dark background (spike count 2–31, $n = 5$ units) (Figs. 3b, 4). Among the moving stimuli we tested, the whole-field sinusoidal drifting grating (stimulus S5) elicited the weakest response (spike count 0–5, $n = 5$ units; Figs. 3b, 4). For stationary stimuli, Ipc neurons responded to a whole-field random checkerboard stimulus (spike count 1–29, $n = 5$; Fig. 4) and to a small dark spot flashed at the center of the receptive field (spike count 2–50, $n = 5$ units; Fig. 5). Ipc neurons responded little to whole-field diffuse illumination changes from white to black (spike count 0–5, $n = 5$; data not shown). In conclusion, Ipc neurons respond to a variety of moving or flashing stimuli as long as they are small.

Excitatory receptive field (ERF) structure

We used the results obtained with the small moving black spot (stimulus S1) to elucidate the excitatory receptive field structure of Ipc neurons. An analysis was developed to

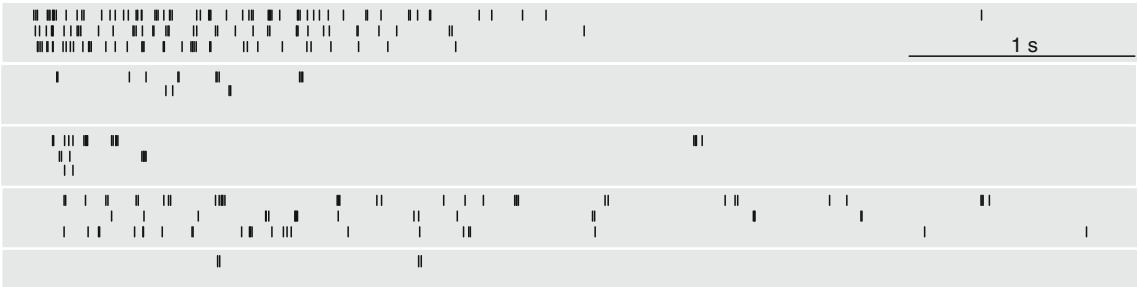

Fig. 5 Adaptation of single-unit Ipc responses to a stationary flash (stimulus S6, see "Methods"). Spike raster ($m = 3$, except bottom unit where $m = 2$) of 5 single-unit Ipc responses (same as in Fig. 4) are shown. Flashing spot size kept constant for one unit but varied slightly (6–8°) from unit to unit. The *gray boxes* indicate the onset and duration of the stimuli

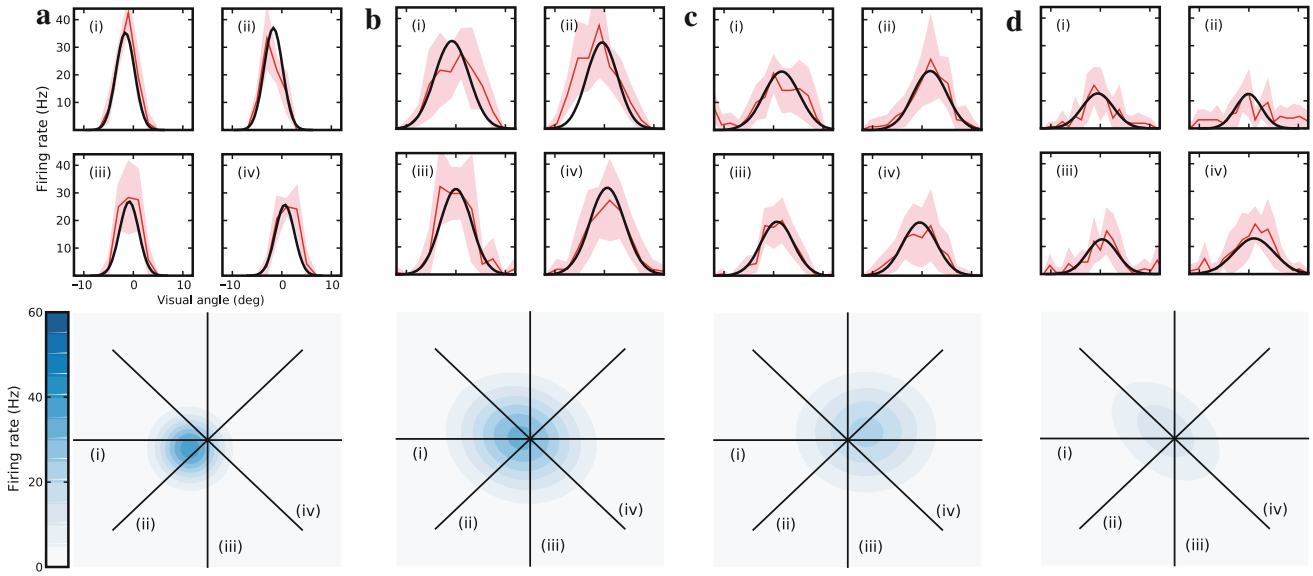

Fig. 6 Two-dimensional shape of the excitatory receptive field, presented for 4 Ipc units (out of the 9 analyzed). For each unit, top four panels show the average firing rate (*red line*) with SD ($m = 3$, *pink*) along four directions, indicated by *Roman numbers*. The *black line* in each panel represents the 2D Gaussian fitting along that direction (see "Methods"). The bottom plot (*blue*) shows the location and size of the Gaussian fit (the contour plot windows are all 22° square). The *scale bar* represents the firing rate. All 4 units are shown in the same scale

measure the gross structure of the ERF even when the location of the ERF center was only estimated during stimulus presentation. Single-unit Ipc responses were collected in response to a small black moving spot (stimulus S1). For each direction, peristimulus time histograms, PSTHs (bin 200 ms, smoothed by 400 ms window) were calculated. The delay due to response latency for each unit was adjusted by overlaying the PSTHs of opposite directions. This delay varied between 100 and 300 ms ($n = 5$ units), which was consistent with the response delay obtained from flashing small dark spots at the center of the receptive field of recorded units. The PSTHs were averaged over multiple trials and translated into 2D spatial coordinates in accordance with the stimulus. These data suggested a 2D Gaussian shape. By taking slices of a 2D Gaussian surface and comparing with the spike histograms, we were able to fit 2D Gaussian to each unit. A genetic algorithm (Druckmann et al. 2008) was utilized to determine the best position, height, widths, and orientation angle of the 2D Gaussian functions, by minimizing the squared difference between the 2D Gaussian function and the data (Fig. 6, top panels, red: average rate; pink: SD; black: Gaussian fit). This method enabled us to reproduce the ERF structure (Fig. 6, bottom panels) even if the spot missed the exact center (e.g. Fig. 6a). For the 9 units analyzed, the half-widths (half-width 1: Avg. 2.4°, SD 0.6; half-width 2: Avg. 2.9°, SD 0.8) of the 2D Gaussian fits (Fig. 6, bottom panels) did not differ significantly. This indicates that Ipc neurons have spatially restricted excitatory receptive fields with circular structure.

Stimulus–response profile

We studied responses of the Ipc neurons to different sizes of black moving spots (Fig. 7a). For each spot size, the stimulus moved in eight directions (stimulus S1) through the center of the stimulus coordinate system tracing the Ipc excitatory receptive field. The firing rates along all eight directions were calculated by dividing the total spike count along one direction by half of the stimulus duration. To avoid any artifact due to missing the center of the Ipc ERF along any one direction, the maximum value of average firing rates among eight directions was chosen to represent the corresponding spot size. Spot size zero corresponded to the average response to the white screen. Single-unit Ipc responses ($n = 4$) followed a classic response-size profile that increased up to a certain spot size then asymptotically decreased to a certain value with increasing of spot size. For the 4 units tested, the Ipc neurons showed a strong spiking response for a spot of radius of about 3°–5° of visual angle (Fig. 7b). The response decreased considerably with increasing spot radius (>5°) for 3 out of 4 units (except the blue unit, Fig. 7b). For the 4 units studied, the firing rate decrease with increasing spot size was independent of direction of stimulus movement. To quantify this response-size profile, we fitted the phenomenological Difference-of-Gaussian model with four independent variables (see "Methods") to these data (lines in Fig. 7b). For three units, the half-widths of the fitted excitatory and inhibitory receptive fields varied between 1°–2° and 3°–5°, respectively. This estimate of the excitatory receptive field

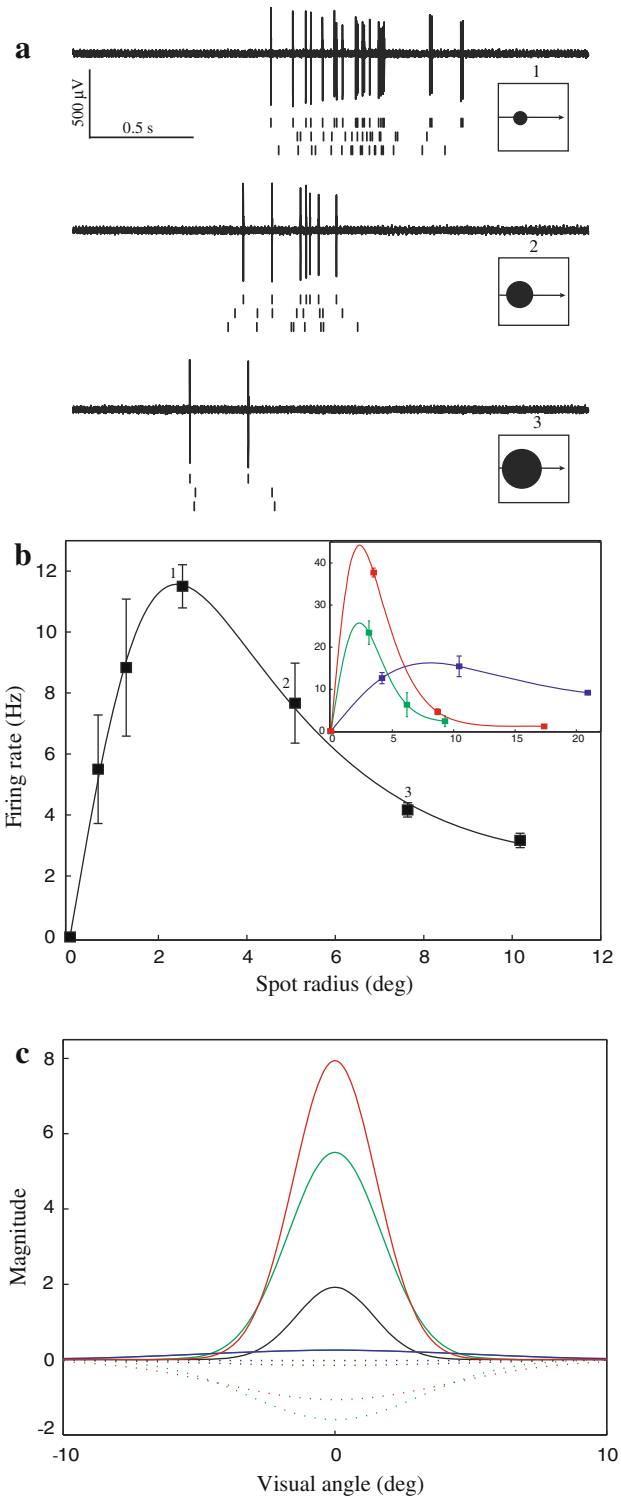

Fig. 7 Ipc responses vary with the size of a small moving black stimuli. **a** The Ipc responses are shown for different spot radii of 2.5°, 5° and 7.5° as the spot moves 9.5°/s along the visual streak through the estimated center of the Ipc excitatory receptive field. For each spot size, one raw voltage trace and three raster plots are shown. The spot size is scaled to the stimulus coordinate system (*square box*) in the drawn stimuli. **b** The response-size profile is shown for the same unit. A difference of Gaussian model is fitted to the result. *Numbers* indicate the average firing rate corresponding to spot radius shown in (**a**). *Inset* Population study of single-unit Ipc responses (3 units) are shown for varying spot radius and fitted with Difference of Gaussian model. *Error bars* indicate the standard deviation between multiple trials ($m = 3$). Speed kept constant for each unit but ranged from 5.5 to 9.5°/s. **c** The excitatory (*solid*) and inhibitory (*dotted*) Gaussians fitted to the response-size profiles of the units in (**b**) from the Difference of Gaussian model (same color-coded)

half-width is consistent with the results obtained using the previous analysis (Fig. 6). The unit with the largest ERF (5°; blue unit of Fig. 7b) also had the weakest surround inhibition. Overall the excitatory receptive field turned out to be narrower and stronger than the overlapping wider and weaker inhibitory receptive field for all 4 units (Fig. 7c).

Direction tuning

To investigate the potential directional sensitivity of Ipc neurons, a small black moving spot (stimulus S1) was used as it elicited the strongest firing in Ipc neurons. Directional preferences to movement along each radial axis were calculated using directional sensitivity index (DSI).

$$\mathrm{DSI} = \frac{R_{\max} - R_{\min}}{R_{\max} + R_{\min}}$$

where $R_{\max}$ and $R_{\min}$ are the higher and lower average firing rates, respectively, recorded during the presentation of the stimulus (stimulus S1) along two opposite directions. By convention, units are classified as directionally sensitive, when $R_{\max} \geq 2R_{\min}$ (i.e. DSI $\geq$ 0.33) (Rosenberg and Ariel 1991; Sato et al. 1995). Opposite directions (such as 0°, 180° etc.) were evaluated together as directional pairs. Since the spot moved along eight directions with 45° separations, each unit produced four directional pairs. The DSI was calculated for total of 36 directional pairs ($n = 9$ units, Fig. 8). We found that the DSI of all but one of the pairs fell below the criterion of 0.33, and thus were not considered directionally sensitive. The absolute values of $R_{\max}$ and $R_{\min}$ were plotted for each unit. The distribution, though above the $R_{\max} = R_{\min}$ line by definition, did not exceed the DSI criterion line of $R_{\max} = 2R_{\min}$, indicating no directional tuning (Fig. 8, inset).

Speed tuning

The speed tuning of Ipc units was also investigated with a small moving spot (stimulus S1). A medium-sized spot (8°–9° of visual angle) that elicited strong spiking activity was moved with different speeds across the RF. For the 2 units studied, speeds up to a certain value elicited similar responses (8–15°/s in Figs. 9a, 3–7°/s in Fig. 9b), whereas the response decreased for higher speed (27°/s in Fig. 9a, 17°/s in 9b). The speed tuning curves of both the units

show a peaked response profile (Fig. 9c, d). For higher speeds, both units responded with a larger delay compared with the response latency for slower speeds. Speed analyses were carried out for all eight different directions of motion for each unit. The results were independent of the direction of spot movement.

Synaptic projection from Imc to Ipc is inhibitory

The Ipc response-size profile suggested the involvement of inhibition in shaping Ipc visual responses. One source for inhibition is the GABAergic Imc neuron. Imc neurons receive broad tectal input and innervate the Ipc, so are well-suited to provide large-field inhibition to Ipc neurons. To test this possibility, we conducted whole-cell blind-patch recordings from Ipc neurons while stimulating the Imc axons in the deep tectal layers. A stimulus electrode (red vertical line, Inset Fig. 10) was lowered into deep tectal SGC layers (~500 μm below the surface) to stimulate Imc axons antidromically. The resulting Imc spikes traveled from the optic tectum to the Imc and continued to the Ipc. Because of the broad and dense Imc projection pattern, a recorded Ipc neuron (blue dot) had a high probability of receiving synaptic inputs from the stimulated Imc axons (see Fig. 1). To avoid direct stimulation of the Ipc axon of the recorded neuron or SGP neurons, the topography of Ipc-tectum projection was taken into account (Sereno and Ulinski 1987) and recordings were made from the dorso-lateral part of the Ipc while stimulating the rostro-medial tectum. Six Ipc neurons had response latencies less than 10 ms which is consistent with antidromic Imc axon stimulation and displayed substantial long-lasting (200–400 ms) inhibition. Additionally, there were three cells investigated by this stimulation protocol that were excluded. Among them, two cells showed long inhibition but were excluded from the analysis because of their longer response latencies, which indicate an indirect activation of the Imc neurons. In one cell, the deep tectal stimulation showed long inhibition along with short excitation, which is consistent with stimulation of both GABAergic Imc and glutamatergic SGP neurons in deep tectal layers. To determine the source of this inhibitory current, current clamp experiments were conducted (Fig. 10). The inhibitory post synaptic potential due to Imc stimulation reversed at around −79 mV (Fig. 10, bottom).

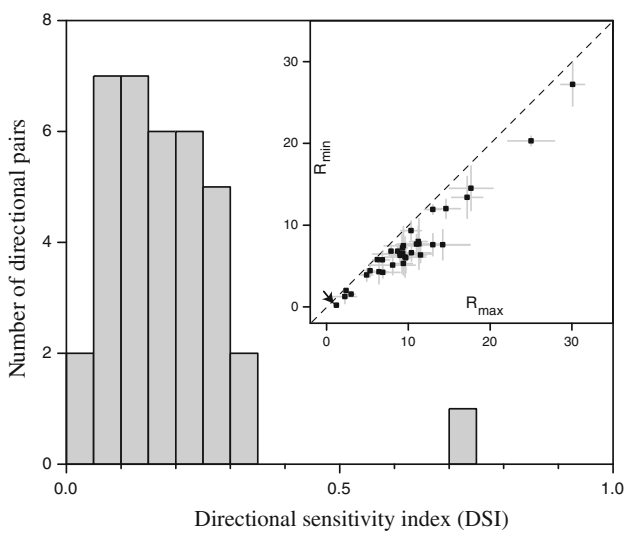

Fig. 8 Histogram distribution of the directional sensitivity index (DSI, see "Methods") is plotted for 36 directional pairs from 9 single-unit Ipc neurons (nine recording sites, eight brains). The spot diameter and speed are kept constant for multiple trials in each unit but varied slightly between different units (diameter 5–9°, speed 6–10°/s using stimulus S1). DSI index of all but one pair falls below 0.33. *Inset* R_{max} and R_{min} for all the directional pairs are plotted with their absolute value of firing rate (Hz) with SD (*gray bars*). R_{max} and R_{min} represent the average value of the higher and lower firing rates over multiple trials ($n = 3$) for each directional pair. The dotted line represents $R_{max} = R_{min}$. The *arrow* indicates the directional pair with lowest firing rate that has a DSI just above the criterion

Discussion

We show that turtle Ipc neurons have a localized excitatory receptive field with surround inhibition, a preference for small stimuli, as well as significant adaptation to static stimuli. Here, we compare our findings with those from other animals, discuss possible mechanisms based on our results and the underlying circuitry of the system, and provide an outlook for the role of Ipc cholinergic feedback for tectal visual processing in turtle.

The small moving stimuli generate vigorous spiking responses in the turtle Ipc neurons as well as in isthmic neurons of many species (pigeon: Yan and Wang 1986; Wang and Frost 1991; Marín et al. 2005; Maczko et al. 2006; Li et al. 2007; Marín et al. 2007; fish: Gallagher and Northmore 2006; cat: Sherk 1979a). The spontaneous firing rates of turtle Ipc neurons and pigeon's nucleus isthmi cells are found to be low (Wang and Frost 1991) compared with the high spontaneous activity of parabigeminal (PBN) neurons (Sherk 1979a; Cui and Malpeli 2003; Goddard et al. 2007). We have found that the turtle Ipc neurons are not directionally sensitive (Fig. 8), which is consistent with the weakly directionally sensitive pigeon Ipc neurons (Wang and Frost 1991; Li et al. 2007) and cat PBN neurons (Sherk 1979a). However, evidence of directional selectivity of isthmic neurons has been found in other species (reptile: Wang et al. 1983; bird: Yan and Wang 1986). We have found oscillatory bursts in the turtle Ipc neurons in response to visual stimulation (Fig. 3a), which has also been observed in avian Ipc neurons (Marin et al. 2005, 2007) and fish isthmic neurons (Northmore and Gallagher

2003). Visual response habituation has been observed in nucleus isthmi and optic tectum of teleosts (Northmore and Gallagher 2003). Habituation is also present in neurons in bird optic tectum (Marín et al. 2005; Mysore et al. 2010). The temporal adaptation with considerable variability in time-course from unit to unit is prominent in bird Ipc neurons while responding to a small bright spot stimulus (Maczko et al. 2006). Another similarity we observed with isthmic neurons of other species is their broad speed tuning (turtle: Fig. 9; bird: Wang and Frost 1991; cat: Sherk 1979a).

The turtle Ipc excitatory receptive field is shaped in the pathway from retina, to tectum, to Ipc. The radial narrow dendrites of the tectal SGP neurons overlap with retinal axon terminals in superficial tectal layers (Kunzle and Schnyder 1984). In turn, axons from the SGP neurons project to the ipsilateral Ipc in a topographic fashion (Fig. 1). The SGP apical radial dendrites form dendro-dendritic synapses within the SFGS layer (Schechter and Ulinski 1979), thus providing the hardware for the lateral spread of local retinal inputs and suggesting broad Ipc receptive fields. Yet, our recordings reveal circular excitatory Ipc receptive fields of Gaussian shape with an average half-width just below 3°. Neurons in cat PBN have a similar excitatory receptive field with a little less than 3° in diameter (Sherk 1979a). In contrast, pigeon Ipc neurons have circular excitatory receptive fields with diameters in the range from 10 to 20° (Marin et al. 2005, 2007; Li et al. 2007) and the excitatory receptive fields of frog nucleus isthmi neurons are even larger (Winkowski and Gruberg 2002; Caudill et al. 2010).

To determine the inhibitory receptive field structure of Ipc neurons, we investigated the Ipc response-size profile using different spot sizes (Fig. 7). Based on a Difference-of-Gaussian analysis the inhibitory receptive field turned out to be weaker and about twice as big as the excitatory receptive field of Ipc neurons. This stimulus size tuning, which is the result of a surround inhibition, is found in cat PBN (Sherk 1979a), bird Ipc (Wang and Frost 1991), and tectal (Mysore et al. 2010) neurons. A similar response-size profile can also be observed in the LGN (Sillito and Jones 2002; Alitto and Usrey 2003) and cortical VI neurons (Sceniak et al. 1999).

In the turtle isthmotectal system, the GABAergic Imc neuron is a likely candidate for the generation of this inhibitory surround through its broad projection to the Ipc. Consistent with this hypothesis, we have found that the Imc-Ipc synapses are inhibitory (Fig. 10). In addition, retinal and tectal processing (Bowling 1980; Granda and Fulbrook 1989) may contribute to the Ipc's visual response properties. Our study cannot separate these influences from the role of Imc neurons in providing inhibition to the Ipc neurons.

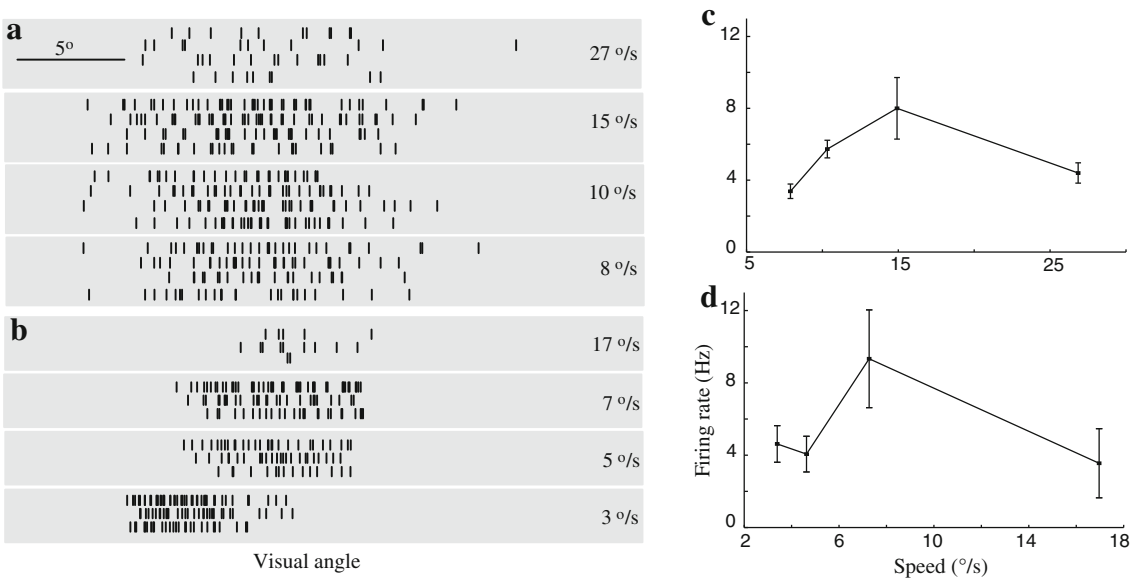

Fig. 9 Variation of Ipc response with different speeds of small black moving stimuli (stimulus S1, see "Methods"). Spikes are plotted at the position they occurred in the receptive field for different speeds with a response latency of 300 ms. Each *gray box* represents 30° of visual angle. Shown are each cell's strongest response among all eight directions presented. **a** Raster of four trials is shown for a moving spot of diameter 9° with different speed values (mentioned at the far right). For different speeds the average spike count and SD values are (format: Speed, Mean ± SD); 27°/s, 11 ± 1.6; 15°/s, 36 ± 8.9; 10°/s, 37.2 ± 3.7; 8°/s, 28.8 ± 3.9. **b** Raster of three trials are shown for a different unit for a spot (diameter 8°) moving with different speeds (similar to 9**a**). The mean and SD values of spike count for different speeds are 17°/s, 5.3 ± 3.5; 7°/s, 32.7 ± 11.6; 5°/s, 22.3 ± 6.7; 3°/s, 34.7 ± 9.3. **c** Speed tuning plot of the unit presented in (**a**). The firing rate is calculated by dividing the total number of spikes by the duration of the stimulus movement. *Error bars* represent SD. **d** Speed tuning plot of the unit shown in (**b**)

The feedback pathway from nucleus isthmi to tectum in turtle consists of (Fig. 1) a narrow, topographic, cholinergic projection to multiple tectal layers from Ipc neuron and a broad, inhibitory projection from Imc neuron to deep tectal layers (Sereno and Ulinski 1987). This anatomical connection underscores the fact that the cholinergic feedback mediated by Ipc neurons at one tectal locus faces competition with feedback produced at other tectal loci via long distance suppression by Imc neurons. These interactions might provide spatially specific modulation of tectal circuitry and mediate mechanisms of visual processing in the tectofugal pathway in different species (Gruberg et al. 2006).

The cholinergic Ipc projections also play an important role in upstream visual processing in the tectofugal pathway. Large-field neurons in the SGC layer of the turtle tectum project to the nucleus rotundus in a non-topographic manner, forming a key element of tectofugal pathway (Reiner 1994; Belekova et al. 2003). The tectal SGC neurons' dendritic branches extend into the superficial retinorecipient tectal layers (SFGS). The topographically organized columnar Ipc axon terminals spatially overlap with the RGC axons and the SGC dendrites. Thus, the release of ACh from Ipc axon terminals across several tectal layers provides ample potential for a spatially specific cholinergic modulation of retino-tectal synaptic transmission and in turn, the ascending visual pathway. This conjecture is supported by the observations that isthmic activity enhances calcium influx into the optic nerve fiber terminals in frog (Dudkin and Gruberg 2003) and by

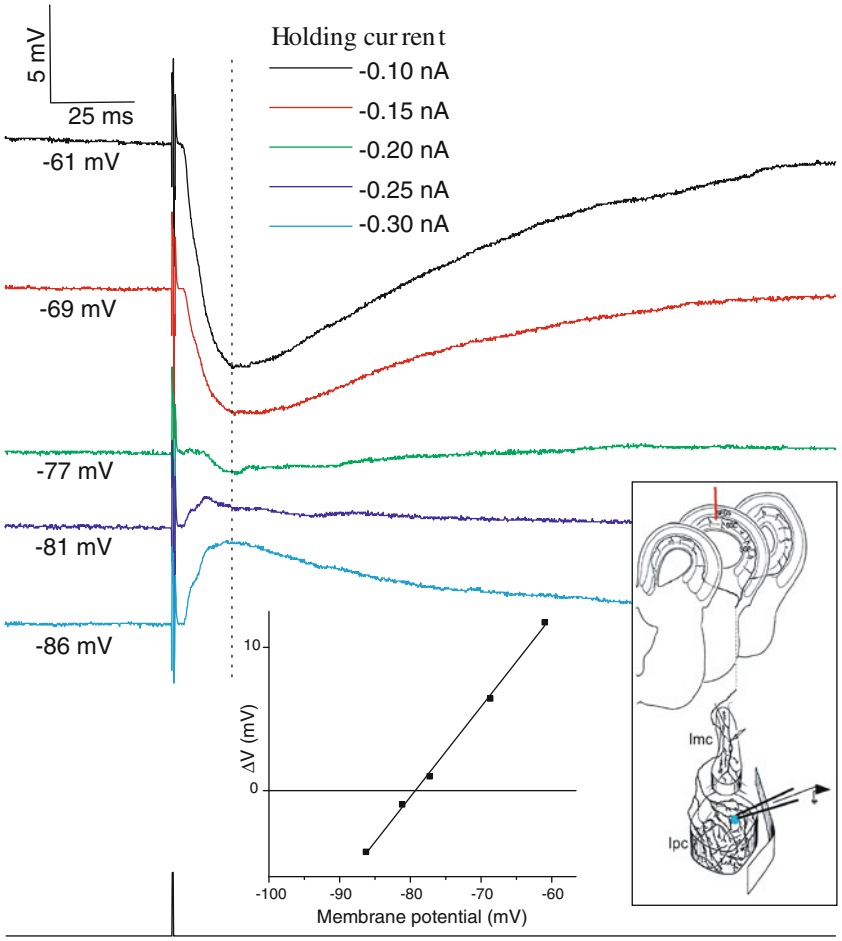

Fig. 10 Synaptic response of an Ipc neuron to deep tectal stimulation, presumably activating Imc axons directly. Single pulse stimulation (0.5 ms, 200 μA) resulted in a long-lasting postsynaptic potential (PSP). Recordings were obtained for five different holding currents corresponding to membrane potentials between −61 and −86 mV. Each *trace* represents an average of three trials. The peak amplitude of the PSP, ΔV, was measured as the difference between the membrane potential at the holding current and the membrane potential at 18 ms after the stimulus pulse (*vertical dotted* line). The PSP peak amplitude increases linearly with increasing membrane potential and reverses sign at −79 mV. *Inset* Schematic of stimulating electrode in tectum (*red line*) and recording from an Ipc neuron (*blue dot*). The GABAergic Imc neuron's axon splits into two major branches. One branch projects nontopographically to the Ipc and the other branch projects nontopographically to tectal layers SGC and SGP. The two isthmic nuclei have been enlarged relative to the tectum for clarity. The axon split and the broad projection pattern allows for Imc stimulation via its axons in the tectum. *Inset* reproduced from Sereno and Ulinski (1987) with additions

findings that the local inactivation of the Ipc prevents visual responses in the spatially corresponding ascending RGC-SGC visual pathway to the nucleus rotundus in birds (Marín et al. 2007). Clearly, a deeper understanding of the Ipc visual responses will be a prerequisite for gaining insight into the role of spatiotemporal ACh release for visual processing in the optic tectum or superior colliculus.

Acknowledgments This study was supported by National Eye Institute Grant R01 EY-18818 to R. Wessel. We thank Matthew Caudill for critical reading of early versions of the manuscript. All surgical procedures used in this study were approved by the Washington University Institutional Animal Care and Use Committee and conform to the guidelines of the National Institutes of Health on the Care and Use of Laboratory Animals.

References

Alitto HJ, Usrey WM (2003) Corticothalamic feedback and sensory processing. Curr Opin Neurobiol 13:440–445

Ariel M, Kogo N (2001) Direction tuning of inhibitory inputs to the turtle accessory optic system. J Neurophysiol 86:2919–2930

Belekova M, Kenigfest N, Rio JP, Reperant J, Ward R, Vesselkin N, Karamian O (2003) Tectothalamic visual projections in turtles: their cells of origin revealed by tracing methods. J Comp Neurology 457:37–56

Bowling DB (1980) Light responses of ganglion cells in the retina of the turtle. J Physiol 299:173–196

Brown KT (1969) A linear area centralis extending across the turtle retina and stabilized to the horizon by non-visual cues. Vis Res 9:1053–1062

Caudill MS, Eggebrecht AT, Gruberg ER, Wessel R (2010) Electrophysiological properties of isthmic neurons in frogs revealed by in vitro and in vivo studies. J Comp Physiol A 196:249–262

Cui H, Malpeli JG (2003) Activity in the parabigeminal nucleus during eye movements directed at moving and stationary targets. J Neurophysiol 89:3128–3142

DeAngelis GC, Freeman RD, Ohzawa I (1994) Length and width tuning of neurons in the cat's primary visual cortex. J Neurophysiol 71:347–374

Desan PH, Gruberg ER, Eckenstein F (1984) A cholinergic projection from the nucleus isthmi to the optic tectum in turtle and frog. Proc Soc Neurosci 10:575 (abstract)

Druckmann S, Berger TK, Hill S, Schürmann F, Markram H, Segev I (2008) Evaluating automated parameter constraining procedures of neuron models by experimental and surrogate data. Biol Cybern 99:371–379

Dudkin EA, Gruberg ER (2003) Nucleus isthmi enhances calcium influx into optic nerve fiber terminals in *Rana pipiens*. Brain Res 969:44–52

Dudkin EA, Sheffield JB, Gruberg ER (2007) Combining visual information from the two eyes: the relationship between isthmotectal cells that project to ipsilateral and to contralateral optic tectum using fluorescent retrograde labels in the frog, *Rana pipiens*. J Comp Neurol 502:38–54

Gallagher SP, Northmore DP (2006) Responses of the teleostean nucleus isthmi to looming objects and other moving stimuli. Vis Neurosci 23:209–219

Goddard CA, Knudsen EI, Huguenard JR (2007) Intrinsic excitability of cholinergic neurons in the rat parabigeminal nucleus. J Neurophysiol 98:3486–3493

Granda AM, Fulbrook JE (1989) Classification of turtle retinal ganglion cells. J Neurophysiol 62:723–737

Graybiel AM (1978) A satellite system of the superior colliculus: the parabigeminal nucleus and its projection to the superficial collicular layers. Brain Res 145:365–374

Gruberg ER, Udin SB (1978) Topographic projections between the nucleus isthmi and the tectum of the frog, *Rana pipiens*. J Comp Neurol 179:487–500

Gruberg ER, Dudkin EA, Wang Y, Marin G, Salas C, Sentis E, Letelier JC, Mpodozis J, Malpeli J, Cui H, Ma R, Northmore D, Udin S (2006) Influencing and interpreting visual input: the role of a visual feedback system. J Neurosci 26:10368–10371

Hall WC, Fitzpatrcik D, Klatt LL, Raczkowski D (1989) Cholinergic innervation of the superior colliculus in the cat. J Comp Neurol 287:495–514

Kriegstein AR (1987) Synaptic responses of cortical pyramidal neurons to light stimulation in the isolated turtle visual system. J Neurosci 7:2488–2492

Kunzle H, Schnyder H (1984) The isthmus-tegmentum complex in the turtle and rat: a comparative analysis of its interconnections with the optic tectum. Exp Brain Res 56:509–522

Li DP, Xiao Q, Wang SR (2007) Feedforward construction of the receptive field and orientation selectivity of visual neurons in the pigeon. Cereb Cortex 17:885–893

Lucas-Meunier E, Fossier P, Baux G, Amar M (2003) Cholinergic modulation of the cortical neuronal network. Eur J Physiol 446:17–29

Lucas-Meunier E, Monier C, Amar M, Baux G, Fregnac Y, Fossier P (2009) Involvement of nicotinic and muscarinic receptors in the endogenous cholinergic modulation of the balance between excitation and inhibition in the young rat visual cortex. Cereb Cortex 19:2411–2427

Maczko KA, Knudsen PF, Knudsen EI (2006) Auditory and visual space maps in the cholinergic nucleus isthmi pars parvocellularis of the barn owl. J Neurosci 26:12799–12806

Marín G, Mpodozis J, Sentis E, Ossandón T, Letelier JC (2005) Oscillatory bursts in the optic tectum of birds represent re-entrant signals from the nucleus isthmi pars parvocellularis. J Neurosci 25:7081–7089

Marín G, Salas C, Sentis E, Rojas X, Letelier JC, Mpodozis JA (2007) Cholinergic gating mechanism controlled by competitive interactions in the optic tectum of the pigeon. J Neurosci 27:8112–8121

McCormick DA (1993) Actions of acetylcholine in the cerebral cortex and thalamus and implications for functions. Prog Brain Res 98:303–308

Medina L, Reiner A (1994) Distribution of choline acetyltransferase immunoreactivity in the pigeon brain. J Comp Neurol 342:497–537

Metherate R (2004) Nicotinic acetylcholine receptors in sensory cortex. Learn Mem 11:50–59

Mysore SP, Asadollahi A, Knudsen EI (2010) Global inhibition and stimulus competition in the owl optic tectum. J Neurosci 30:1727–1738

Northmore DP (1991) Visual responses of nucleus isthmi in a teleost fish (*Lepomis macrochirus*). Vision Res 31:525–535

Northmore DP, Gallagher SP (2003) Functional relationship between nucleus isthmi and tectum in teleosts: synchrony but no topography. Vis Neurosci 20:335–348

Northmore DP, Granda AM (1991) Ocular dimensions and schematic eyes of freshwater and sea turtles. Vis Neurosci 7:627–635

Peirce JW (2008) Generating stimuli for neuroscience using PsychoPy. Front Neuroinformatics 2:10

Powers AS, Reiner A (1993) The distribution of cholinergic neurons in the central nervous system of turtles. Brain Behav Evol 41:326–345

Quiroga RQ, Nadasdy Z, Ben-Shaul Y (2004) Unsupervised spike detection and sorting with wavelets and superparamagnetic clustering. Neural Comput 16:1661–1687

Reiner A (1994) Laminar distribution of the cells of origin of ascending and descending tectofugal pathways in turtles: implications for the evolution of tectal lamination. Brain Beh Evol 43:254–292

Rodieck RW (1965) Quantitative analysis of cat retinal ganglion cell response to visual stimuli. Vision Res 5:583–601

Rosenberg AF, Ariel M (1990) Visual-response properties of neurons in turtle basal optic nucleus in vitro. J Neurophysiol 63:1033–1045

Rosenberg AF, Ariel M (1991) Electrophysiological evidence for a direct projection of direction-sensitive retinal ganglion cells to the turtle's accessory optic system. J Neurophysiol 65:1022–1033

Sato H, Katsuyama N, Tamura H, Hata Y, Tsumoto T (1995) Mechanisms underlying direction selectivity of neurons in the primary visual cortex of the macaque. J Neurophysiol 74:1382–1394

Sceniak MP, Ringach DL, Hawken MJ, Shapley R (1999) Contrast's effect on spatial summation by macaque V1 neurons. Nat Neurosci 2:733–739

Schechter Pb, Ulinski PS (1979) Interactions between tectal radial cells in the red-eared turtle, *Pseudemys scripta Elegans*: an analysis of tectal modules. J Morph 162:17–36

Sereno MI, Ulinski PS (1987) Caudal topographic nucleus isthmi and the rostral nontopographic nucleus isthmi in the turtle, *Pseudemys scripta*. J Comp Neurol 261:319–346

Sherk H (1978) Visual response properties and visual field topography in the cat's parabigeminal nucleus. Brain Res 145:375–379

Sherk H (1979a) A comparison of visual-response properties in cat's parabigeminal nucleus and superior colliculus. J Neurophysiol 42:1640–1655

Sherk H (1979b) Connections and visual field mapping in cat's tectoparabigeminal circuit. J Neurophysiol 42:1656–1668

Sillito AM, Jones HE (2002) Corticothalamic interactions in the transfer of visual information. Philos Trans R Soc Lond B Biol Sci 357:1739–1752

Sorenson EM, Parkinson D, Dahl JL, Chiappinelli VA (1989) Immunohistochemical localization of choline acetyltransferase in the chicken mesencephalon. J Comp Neurol 281:641–657

Wang SR (2003) The nucleus isthmi and dual modulation of the receptive field of tectal neurons in non-mammals. Brain Res Rev 41:13–25

Wang YC, Frost BJ (1991) Visual response characteristics of neurons in the nucleus isthmi magnocellularis and nucleus isthmi parvocellularis of pigeons. Exp Brain Res 87:624–633

Wang SR, Yan K, Wang YT, Jiang SY, Wang XS (1983) Neuroanatomy and electrophysiology of the lacertilian nucleus isthmi. Brain Res 275:355–360

Wang SR, Wang YC, Frost BJ (1995) Magnocellular and parvocellular divisions of pigeon nucleus isthmi differentially modulate visual responses in the tectum. Exp Brain Res 104:376–384

Wang Y, Xiao J, Wang SR (2000) Excitatory and inhibitory receptive fields of tectal cells are differentially modified by magnocellular and parvocellular divisions of the pigeon nucleus isthmi. J Comp Physiol A 186:505–511

Wang Y, Major DE, Karten HJ (2004) Morphology and connections of nucleus isthmi pars magnocellularis in chicks (*Gallus gallus*). J Comp Neurol 469:275–297

Wang Y, Luksch H, Brecha NC, Karten HJ (2006) Columnar projections from the cholinergic nucleus isthmi to the optic tectum in chicks (*Gallus gallus*): a possible substrate for synchronizing tectal channels. J Comp Neurol 494:7–35

Wiggers W, Roth G (1991) Anatomy, neurophysiology and functional aspects of the nucleus isthmi in salamanders of the family Plethodontidae. J Comp Physiol A 169:165–176

Winkowski DE, Gruberg ER (2002) The representation of the ipsilateral eye in nucleus isthmi of the leopard frog, *Rana pipiens*. Vis Neurosci 19:669–679

Yan K, Wang SR (1986) Visual responses of neurons in the avian nucleus isthmi. Neurosci Lett 64:340–344